ACS APPLIED ELECTRONIC MATERIALS

pubs.acs.org/acsaelm Article

Graphene Nanoribbon Field-Effect Transistors with Top-Gate Polymer Dielectrics

Beomjin Jeong,[#] Michael Wuttke,[#] Yazhou Zhou, Klaus Müllen, Akimitsu Narita, and Kamal Asadi*

Cite This: *ACS Appl. Electron. Mater.* 2022, 4, 2667−2671 Read Online

ACCESS | Metrics & More | Article Recommendations | Supporting Information

ABSTRACT: Graphene nanoribbons (GNRs) have demonstrated great potential for nanoscale devices owing to their excellent electrical properties. However, the application of the GNRs in large-scale devices still remains elusive mainly due to the absence of facile, nonhazardous, and nondestructive transfer methods. Here, we develop a simple acid (HF)-free transfer method for fabricating field-effect transistors (FETs) with a monolayer composed of a random network of GNRs. A polymer layer that is typically used as mechanical support for transferring GNR films is utilized as the gate dielectric. The resultant GNR-FETs exhibit excellent FET characteristics with a large on/off switching current ratio of >10^4. The transfer process enables the demonstration of the first GNR-based nonvolatile memory. The process offers a simple route for GNRs to be utilized in various optoelectronic devices.

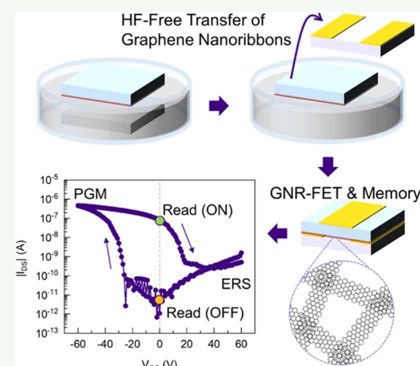

KEYWORDS: *9-armchair graphene nanoribbons, wet-etch transfer, ferroelectric polymers, field-effect transistors, memory*

■ INTRODUCTION

Carbon-based semiconductors, such as conjugated polymers, small organic molecules, and graphene, have been extensively investigated for various applications such as mechanically flexible/wearable electronics, displays, and chemical and biological sensors.[1−3] Graphene is a two-dimensional (2D) conjugated system that has no band gap but shows remarkably high charge carrier mobilities, whereas conjugated semiconductors possess a band gap but show limited charge transport.[4,5] Graphene nanoribbons (GNRs) bridge the two classes of materials and have been of great interest because GNRs possess finite electronic band gaps due to the quantum confinement of charge carriers and edge effects.[6−9]

Bottom-up synthetic routes, wherein atomically thin monolayers of a random network of GNRs are grown on metallic catalysts (e.g., Au on a mica substrate), can yield a monolayer film of a dense network of GNRs.[10,11] Following the growth, the GNR film should be detached from the Au/mica substrate and transferred onto a target substrate for device fabrication. The common procedure is the wet-etch transfer method, where Au is removed with etchants. However, the wet-etch transfer method involves the use of a hazardous acid, namely HF to remove the mica substrate.[12] Moreover, a polymer support layer such as poly(methyl methacrylate) (PMMA) is needed to avoid breaking the mechanically fragile GNR/Au film during the wet-etch transfer process.[12] The polymer support layer is normally removed through several washing steps to ensure no residuals on the GNR film, which makes the procedure complicated. Furthermore, the removal of the support layer can lead to unintentional removal of the ribbons and therefore physically damage the GNR film.[13] Simple, nonhazardous, and nondestructive transfer methods would be therefore of advantage for the fabrication of GNR-based electronic devices.

Here, we report a simplified wet-etch transfer process for GNR-FETs wherein the support layer is used as the dielectric in a top-gated FET configuration. Hence, the transfer process does not involve the removal of the polymer support layer, yielding a simplified and nondestructive fabrication process. The GNR/polymer bilayer film can be easily detached from a growth substrate through conventional KI/I_2 etchant, without the use of HF, and transferred to a target substrate for device integration. The GNR-FETs are realized using a poly(vinylidene fluoride-*co*-trifluoroethylene-*co*-chlorofluoroethylene) [P(VDF-TrFE-CFE)] as the polymeric transfer layer. P(VDF-TrFE-CFE) is a high-*k* polymer dielectric, and the fabricated GNR-FET thereof exhibits decent FET characteristics such as a high on/off ratio of >10^4. We further demonstrate that a nonvolatile GNR-FET memory can also be fabricated by simply changing the support layer to a ferroelectric polymer such as poly(vinylidene fluoride-*co*-trifluoroethylene) [P(VDF-TrFE)]. The resultant GNR-FET

Received: February 10, 2022
Accepted: May 12, 2022
Published: May 26, 2022

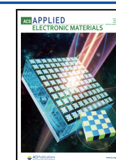

Downloaded via MPI POLYMERFORSCHUNG on July 18, 2022 at 10:38:53 (UTC).
See https://pubs.acs.org/sharingguidelines for options on how to legitimately share published articles.

ACS Publications

© 2022 The Authors. Published by American Chemical Society

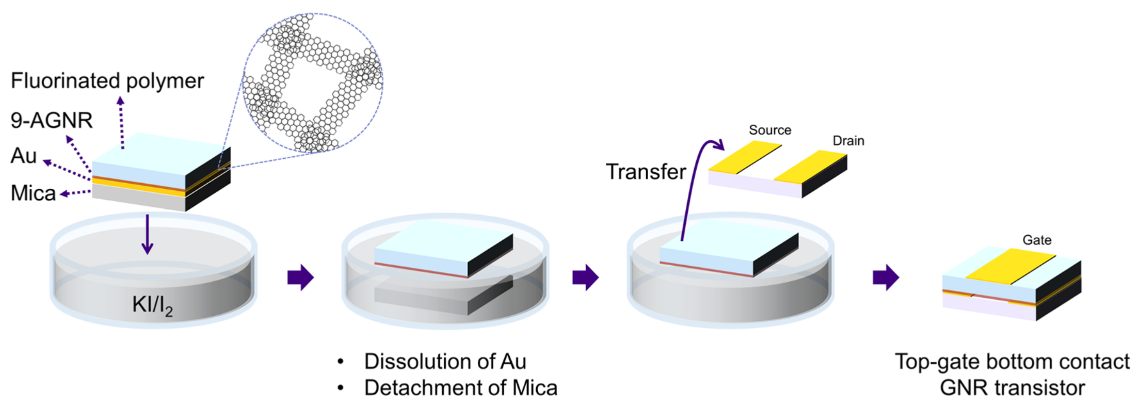

Figure 1. Schematic illustration of the wet-etch transfer method. A fluorinated polymer film coated on the 9-AGNR/Au/mica substrate is floated on a KI/I_2 solution for etching of the Au interlayer. The mica substrate is detached and settled down, leaving the polymer/9-AGNR bilayer film to float on the bath. The polymer/9-AGNR bilayer film is transferred onto the prepatterned source/drain substrate. Finally, a gate electrode is deposited on top.

memory exhibits resistance switching with a high on/off ratio of $>10^4$ at zero gate bias, long data retention time, and high cycle endurance.

EXPERIMENTAL SECTION

Materials. P(VDF-TrFE-CFE) terpolymer with a molar ratio of VDF/TrFE/CFE = 64.8:27.4:7.8 was purchased from Piezotech (Arkema). P(VDF-TrFE) copolymer with a molar ratio of VDF/TrFE = 75:25 was purchased from Solvay. Au (111)/mica substrates (Phasis, Switzerland or Georg Albert, Germany) were used for the growth of 9-AGNRs. Unless otherwise noted, all of the other chemicals were obtained from Aldrich and used as received.

Synthesis of GNRs. The N = 9-armchair GNRs (9-AGNRs) were synthesized by chemical vapor deposition (CVD) using 3′,6′-dibromo-1,1′:2′,1″-terphenyl (DBTP) as the monomeric building block. The Au/mica substrate was loaded in the middle of a one-zone horizontal tube furnace (Nabertherm, RT 80-250/11S). The tube furnace was heated to 200 °C using a heating belt (Thermocoax Isopad S20) under Ar (500 sccm) and H_2 (100 sccm) gas flows. In the meantime, the monomer of DBTP was sublimed at 145 °C for 20 min to induce dehalogenation and polymerization. The sample was finally annealed at 450 °C for 15 min for intramolecular cyclo-dehydrogenation.

Wet-Etch Transfer Process. The 9-AGNR film grown on the Au/mica substrate was transferred to prepatterned source/drain substrates using P(VDF-TrFE-CFE) or P(VDF-TrFE) polymers as a mechanical support layer. The polymers were dissolved in 2-butanone at a concentration of 60 mg mL^{-1}. The polymer solutions were spin-coated on the 9-AGNR/Au/mica substrate at 2000 rpm for 60 s. The polymer/9-AGNR/Au/mica substrate was floated on a KI/I_2 etchant solution. The mica substrate was detached as the Au interlayer is etched away, leaving the polymer/9-AGNR film floating on the surface of the KI/I_2 solution. After the mica substrate was fully detached, the KI/I_2 bath was changed to water. For HF-assisted transfer, the mica substrate was first etched by HF and, subsequently, Au was removed by the KI/I_2 solution. The polymer/9-AGNR film was washed with water to ensure no residual KI/I_2. After then, the bilayer film was dried at 100 °C for several hours. Finally, the polymer/9-AGNR film was transferred to the prepatterned source and drain electrodes on a SiO_2 substrate.

FET Fabrication. The 9-AGNR FETs were fabricated as a top-gate, bottom-contact configuration. The Au source and drain electrodes (thickness ≈120 nm) with an adhesion layer of Ti (thickness ≈1 nm) were patterned using conventional photo-lithography. The channel length and width were 20 and 6000 μm, respectively. The bilayer of polymer and 9-AGNR films was transferred on top of the source and drain electrodes using the above-mentioned transfer method. The bilayer film was dried at 140 °C for 2 h to remove residual solvents and enhance the crystallization of the polymer dielectric. Finally, a gate electrode of Au (thickness ≈50 nm) was deposited by thermal evaporation using a shadow mask.

Characterization and Measurements. Raman spectra were obtained at a laser excitation wavelength of 532 nm laser for 30 s measuring time. The laser power on the samples was 10 mW. The XPS spectra were acquired from un-monochromatized Mg Kα X-ray lamp (Omicron) and acquired with a hemispherical analyzer (Omicron EA125), with an overall energy resolution of 1.0 eV. Electrical measurements of the FETs were carried out with a Keithley 4200-SCS instrument in a vacuum of 10^{-5} mbar.

RESULTS AND DISCUSSION

Figure 1 represents the device fabrication steps based on the wet-etch transfer process. First, we synthesized N = 9-armchair GNRs (9-AGNRs) through chemical vapor deposition (CVD) under ambient-pressure conditions as previously reported.[14] It has been shown that the resulting 9-AGNR synthesized on an Au/mica substrate exhibits a finite band gap of ≈1.0 eV. A fluorinated polymer, P(VDF-TrFE-CFE) (molar ratio: 64.8−27.4−7.8) or P(VDF-TrFE) (molar ratio: 65−35), is deposited on the 9-AGNR film to mechanically support the network structure of 9-AGNRs during transfer. The polymer/9-AGNR film is detached from the mica substrate by wet-etching of the Au by KI/I_2 solution. This is distinct from the previous method that involved the use of HF to remove the mica substrate before etching gold, thus providing a safer and simplified process for the transfer of CVD-grown GNRs. The polymer/9-AGNR is transferred to a predefined source/drain substrate and finished with the deposition of a gate electrode on top.

The structural integrity of the CVD-synthesized 9-AGNR film has been proved through Raman spectroscopy and X-ray photoelectron spectroscopy (XPS). To characterize 9-AGNR, the top polymer is removed by acetone after transfer. Figure 2a shows the Raman spectra of the 9-AGNR film transferred to a SiO_2 substrate and compares the previous and new methods with or without the step using HF, respectively (see the Supporting Information for the experimental details). The Raman spectra reveal three main peaks at 1251, 1338, and 1602 cm^{-1}, which can be assigned to G and D bands and edge C−H bonds, respectively. These Raman spectra are in excellent agreement with our previous work,[14] demonstrating that the 9-AGNR samples are successfully obtained. The identical Raman peaks for both samples indicate that 9-AGNR

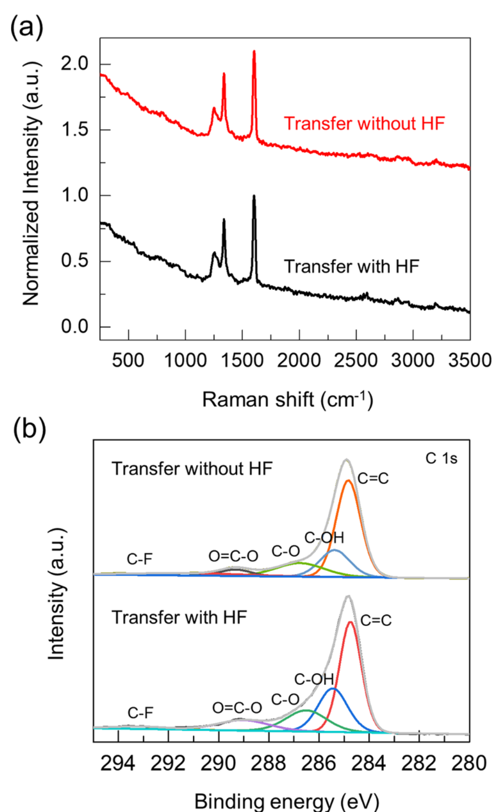

Figure 2. (a) Raman spectra and (b) high-resolution C 1s XPS spectra of the 9-AGNR films transferred to a SiO_2 substrate without HF (top) or with HF (bottom).

is undamaged by the wet-etch transfer process and HF is not requisite for reliably transferring the 9-AGNR film. Figure 2b shows the XPS spectra of the obtained 9-AGNR films. The C 1s spectra demonstrate that 9-AGNR retains its chemical structure with the C═C double bonds of sp^2 hybridization (binding energy = 284.9 eV).[12,14] The XPS spectra further confirm the successful transfer of the 9-AGNR film to a target substrate without HF. The K ions are not detected from the K 2p spectrum, demonstrating that the K ion makes no bonding with 9-AGNRs but simply remains in the etchant solution (Figure S1). The F ions do not remain in the film transferred with HF as confirmed from the comparison of the F 1s spectra with the film transferred without HF (Figure S1). Only a weak signal of F 1s observed in both the films is attributed to the C−F peaks (Figure 2b). Both transfer methods are performed in an aqueous environment. Hence, interfacial water molecules can contribute to C−O or C−OH signals. During the conventional transfer process, the 9-AGNR film is exposed to HF, which causes the formation of the C−F bond, as observed by C−F peaks in the XPS spectrum. The presence of polar C−F bonds promotes surface interaction with polar molecules such as water, thereby producing stronger C−O and C−OH signals in the XPS spectra of 9-AGNR transferred using HF. A weak signal of the I ion is detected from the I 3d spectrum possibly because of the absorption of iodine to the 9-AGNR film from the KI/I_2 etchant solution during the wet-etch transfer (Figure S1).[15] However, the amount the ions is marginal and does not markedly influence the electrical operation of the FETs as we demonstrate next. Finally, the quality of the proposed transfer method has been inspected using optical microscopy and atomic force microscopy (AFM) imaging of the 9-ANGR layer after selective removal of the polymer layer (Figure S2). It is found that the 9-AGNR layer is compact, and its integrity is not affected by the transfer process, although some debris of residual polymers remains. Furthermore, optical microscopy images suggest the absence of notable physical defects and thus robustness of the transfer method.

Figure 3 shows the FET characteristics of the 9-AGNR FET with a P(VDF-TrFE-CFE) gate dielectric. The transfer curve shows a large on/off current ratio of >10^4 with a distinct *p*-type characteristic (Figure 3a). The 9-AGNR FET exhibits an excellent output characteristic with a linear current amplification from V_{GS} = 0 to −60 V at a step of −10 V (Figure 3b). The small hysteresis observed in both FET characteristics is due to the polarization of polar nanodomains in the P(VDF-TrFE-CFE) layer serving as the relaxor in response to the gate bias.[16] The FET mobilities for 9-AGNR extracted from the linear and saturation regimes amount to 2.3×10^{-5} and 4.9×10^{-5} $cm^2\ V^{-1}\ s^{-1}$, respectively. The average mobility is calculated to be 10^{-5} $cm^2\ V^{-1}\ s^{-1}$ with the standard deviation of 5×10^{-6}, which is obtained from 16 devices. It should be noted that the measured mobility for 9-AGNR is a device parameter rather than a material parameter. In large-area devices, the charge carriers must hop from one nanoribbon because the channel consists of a network of randomly oriented 9-AGNRs. The hopping process limits the transport and therefore substantially reduces the mobility.[8] Higher mobilities are expected for longer ribbons or ribbons that are closely packed and well-aligned. Moreover, P(VDF-TrFE-CFE) is a polymer with high relative permittivity (k = 60), which negatively affects the mobility of the semiconductor.[17]

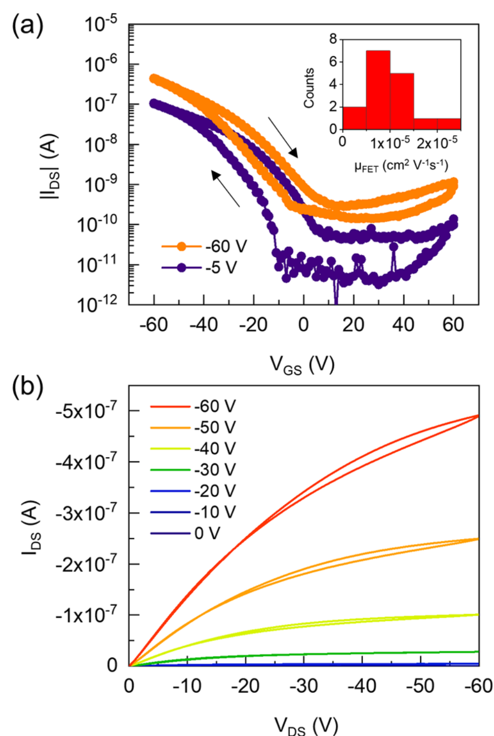

Figure 3. 9-AGNR FET with a P(VDF-TrFE-CFE) gate dielectric. (a) Transfer and (b) output characteristics of the 9-AGNR FET. Inset in (a) shows the statistics of the FET mobility from 16 devices (saturation regime). The average mobility is calculated to be 10^{-5} cm^2 V^{-1} s^{-1} with the standard deviation of 5×10^{-6}.

https://doi.org/10.1021/acsaelm.2c00194
ACS Appl. Electron. Mater. 2022, 4, 2667−2671

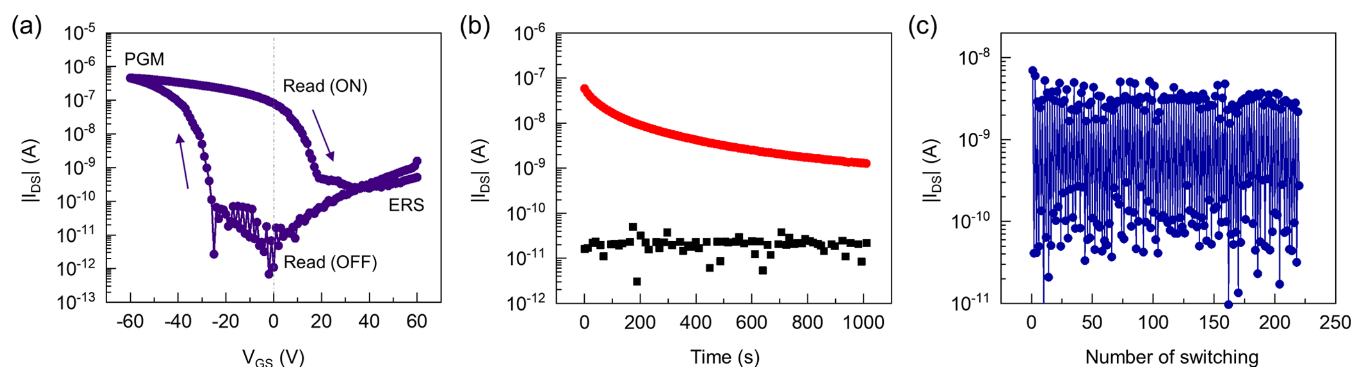

Figure 4. 9-AGNR FET memory with a P(VDF-TrFE) gate dielectric. (a) Transfer characteristic, (b) data retention, and (c) cycle endurance of the 9-AGNR FET memory. The arrows in (a) represent the direction of the measurement. Data retention with time and cycle endurance are measured from a drain current at V_{GS} = 0 V after programming at V_{GS} = −60 V and erasing at V_{GS} = +60 V, respectively.

The devised transfer process provides freedom of choosing the gate dielectric. The polymer support layer can be simply changed depending on the applications. For instance, nonvolatile FET memory can be fabricated using a ferroelectric gate dielectric such as P(VDF-TrFE) as the support layer. P(VDF-TrFE) is a ferroelectric polymer that exhibits bistable polarization programmable by an external electric field.[18] The 9-AGNR FET with the P(VDF-TrFE) gate exhibits large hysteresis in the p-type transfer characteristic arising from the ferroelectric polarization of the P(VDF-TrFE) gate (Figure 4a). As the 9-AGNR exhibits a *p*-type dominant charge transport (Figure 3), hole charge carriers are accumulated at the interface between P(VDF-TrFE) and 9-AGNR upon the application of a negative gate bias higher than a coercive bias of P(VDF-TrFE) (≈−33 V). The negative polarization of P(VDF-TrFE) is compensated by the hole charge carriers, resulting in a high channel conductance (on state) that can be retained even after the removal of an external gate bias. On the other hand, the positive polarization cannot be compensated, and the ferroelectric is depolarized due to the lack of electron charge carriers in the 9-AGNR, giving rise to a low channel conductance (off state). The 9-AGNR FET with the P(VDF-TrFE) gate has bistable current states at V_{GS} = 0 V with an on/off ratio larger than 10^4. The data retention and cycle endurance of the 9-AGNR FET are shown in Figure 4b,c, respectively. The on and off states are programmed by applying V_{GS} = −60 and +60 V, respectively, and then the drain current is probed at V_{GS} = 0 V. The on/off current ratio remains around >10^2 times after 10^3 s. We note that the on state decays relatively fast possibly due to the depolarization of P(VDF-TrFE), whereas the off state remains constant.[19] It should be noted that P(VDF-TrFE) (75−25 molar ratio) has a Curie temperature that is slightly above 100 °C. Therefore, the upper limit for a reliable operation of the GNR FeFET is 100 °C.[20] The upper-temperature limit can be shifted to a higher temperature using polymers with higher Curie temperatures for instanced PVDF homopolymer P(VDF-TrFE) with VDF content higher than 75% or nylon-11.[21,22] It should be noted nevertheless that for many of the envisioned application of flexible electronics, the operating temperature is well below 100 °C, at which the FETs demonstrated here can reliably operate.

■ CONCLUSIONS

In summary, our wet-etch transfer method offers a simplified HF-free route for fabricating thin-film FETs with GNRs using a mechanical support layer as a gate dielectric. The 9-AGNR FETs fabricated by the wet-etch transfer method exhibit excellent FET characteristics with a large on/off switching ratio. A nonvolatile FeFET memory is further demonstrated using a ferroelectric polymer as the support layer. Our process allows GNRs to be utilized in thin-film devices through a simple, nonhazardous, and nondestructive fabrication procedure. Various applications of GNRs are expected in transistor-based thin-film devices for integrated electronics, displays, sensors, etc.

■ ASSOCIATED CONTENT

Supporting Information

The Supporting Information is available free of charge at https://pubs.acs.org/doi/10.1021/acsaelm.2c00194.

High-resolution K 2p, F 1s, and I 3d XPS spectra of the 9-AGNR film (PDF)

■ AUTHOR INFORMATION

Corresponding Author

Kamal Asadi − *Max Planck Institute for Polymer Research, 55128 Mainz, Germany; Department of Physics, University of Bath, Bath BA2 7AY, United Kingdom; Centre for Therapeutic Innovations, University of Bath, Bath BA2 7AY, United Kingdom;* orcid.org/0000-0003-0447-4337; Email: ka787@bath.ac.uk

Authors

Beomjin Jeong − *Max Planck Institute for Polymer Research, 55128 Mainz, Germany; Department of Organic Material Science and Engineering, Pusan National University, Busan 46241, Republic of Korea;* orcid.org/0000-0002-6403-5275

Michael Wuttke − *Max Planck Institute for Polymer Research, 55128 Mainz, Germany*

Yazhou Zhou − *Max Planck Institute for Polymer Research, 55128 Mainz, Germany;* orcid.org/0000-0002-0446-2291

Klaus Müllen − *Max Planck Institute for Polymer Research, 55128 Mainz, Germany; Department of Chemistry, Johannes Gutenberg University Mainz, 55128 Mainz, Germany;* orcid.org/0000-0001-6630-8786

Akimitsu Narita − *Max Planck Institute for Polymer Research, 55128 Mainz, Germany;* orcid.org/0000-0002-3625-522X

Complete contact information is available at:
https://pubs.acs.org/10.1021/acsaelm.2c00194

Author Contributions

[#]B.J. and M.W. contributed equally. The manuscript was written through contributions of all authors. All authors have given approval to the final version of the manuscript.

Funding

Open access funded by Max Planck Society.

Notes

The authors declare no competing financial interest.

ACKNOWLEDGMENTS

This work was financially supported by the Max Planck Society. B.J. and K.A. thank the Alexander von Humboldt Foundation for their financial support. K.M. acknowledges a fellowship from Gutenberg Research College, Johannes Gutenberg University Mainz.

REFERENCES

(1) Torsi, L.; Magliulo, M.; Manoli, K.; Palazzo, G. Organic Field-Effect Transistor Sensors: A Tutorial Review. *Chem. Soc. Rev.* **2013**, *42*, 8612−8628.

(2) Jang, H.; Park, Y. J.; Chen, X.; Das, T.; Kim, M.-S.; Ahn, J.-H. Graphene-Based Flexible and Stretchable Electronics. *Adv. Mater.* **2016**, *28*, 4184−4202.

(3) Anwar, S.; Jeong, B.; Abolhasani, M. M.; Zajaczkowski, W.; Amiria, M. H.; Asadi, K. Polymer Field-Effect Transistor Memory Based on a Ferroelectric Nylon Gate Insulator. *J. Mater. Chem. C* **2020**, *8*, 5535−5540.

(4) Xu, X.; Liu, C.; Sun, Z.; Cao, T.; Zhang, Z.; Wang, E.; Liu, Z.; Liu, K. Interfacial Engineering in Graphene Bandgap. *Chem. Soc. Rev.* **2018**, *47*, 3059−3099.

(5) Li, M.; Mangalore, D. K.; Zhao, J.; Carpenter, J. H.; Yan, H.; Ade, H.; Yan, H.; Müllen, K.; Blom, P. W. M.; Pisula, W.; de Leeuw, D. M.; Asadi, K. Integrated Circuits Based on Conjugated Polymer Monolayer. *Nat. Commun.* **2018**, *9*, No. 451.

(6) Li, X.; Wang, X.; Zhang, L.; Lee, S.; Dai, H. Chemically Derived, Ultrasmooth Graphene Nanoribbon Semiconductors. *Science* **2008**, *319*, 1229−1232.

(7) Llinas, J. P.; Fairbrother, A.; Barin, G. B.; Shi, W.; Lee, K.; Wu, S.; Choi, B. Y.; Braganza, R.; Lear, J.; Kau, N.; Choi, W.; Chen, C.; Pedramrazi, Z.; Dumslaff, T.; Narita, A.; Feng, X.; Müllen, K.; Fischer, F.; Zettl, A.; Ruffieux, P.; Yablonovitch, E.; Crommie, M.; Fasel, R.; Bokor, J. Short-Channel Field-Effect Transistors with 9-Atom and 13-Atom Wide Graphene Nanoribbons. *Nat. Commun.* **2017**, *8*, No. 633.

(8) Richter, N.; Chen, Z.; Tries, A.; Prechtl, T.; Narita, A.; Müllen, K.; Asadi, K.; Bonn, M.; Kläui, M. Charge Transport Mechanism in Networks of Armchair Graphene Nanoribbons. *Sci. Rep.* **2020**, *10*, No. 1988.

(9) Wang, X.; Ouyang, Y.; Li, X.; Wang, H.; Guo, J.; Dai, H. Room-Temperature All-Semiconducting Sub-10-nm Graphene Nanoribbon Field-Effect Transistors. *Phys. Rev. Lett.* **2008**, *100*, No. 206803.

(10) Cai, J.; Ruffieux, P.; Jaafar, R.; Bieri, M.; Braun, T.; Blankenburg, S.; Muoth, M.; Seitsonen, A. P.; Saleh, M.; Feng, X.; Müllen, K.; Fasel, R. Atomically Precise Bottom-Up Fabrication of Graphene Nanoribbons. *Nature* **2010**, *466*, 470−473.

(11) Chen, Z.; Narita, A.; Müllen, K. Graphene Nanoribbons: On-Surface Synthesis and Integration into Electronic Devices. *Adv. Mater.* **2020**, *32*, No. 2001893.

(12) Chen, Z.; Zhang, W.; Palma, C.; Rizzini, A. L.; Liu, B.; Abbas, A.; Richter, N.; Martini, L.; Wang, X.; Cavani, N.; Lu, H.; Mishra, N.; Coletti, C.; Berger, R.; Klappenberger, F.; Kläui, M.; Candini, A.; Affronte, M.; Zhou, C.; Renzi, V. D.; del Pennino, U.; Barth, J. V.; Räder, H. J.; Narita, A.; Feng, X.; Müllen, K. Synthesis of Graphene Nanoribbons by Ambient-Pressure Chemical Vapor Deposition and Device Integration. *J. Am. Chem. Soc.* **2016**, *138*, 15488−15496.

(13) Saraswat, V.; Jacobberger, R. M.; Arnold, M. S. Materials Science Challenges to Graphene Nanoribbon Electronics. *ACS Nano* **2021**, *15*, 3674−3708.

(14) Chen, Z.; Wang, H. I.; Teyssandier, J.; Mali, K. S.; Dumslaff, T.; Ivanov, I.; Zhang, W.; Ruffieux, P.; Fasel, R.; Räder, H. J.; Turchinovich, D.; Feyter, S. D.; Feng, X.; Kläui, M.; Narita, A.; Bonn, M.; Müllen, K. Chemical Vapor Deposition Synthesis and Terahertz Photoconductivity of Low-Band-Gap $N = 9$ Armchair Graphene Nanoribbons. *J. Am. Chem. Soc.* **2017**, *139*, 3635−3638.

(15) Amiri, M. H.; Heidler, J.; Hasnain, A.; Anwar, S.; Lu, H.; Müllen, K.; Asadi, K. Doping Free Transfer of Graphene using Aqueous Ammonia Flow. *RSC Adv.* **2020**, *10*, 1127−1131.

(16) Pramanick, A.; Osti, N. C.; Jalarvo, N.; Misture, S. T.; Diallo, S. O.; Mamontov, E.; Luo, Y.; Keum, J.; Littrell, K. Origin of Dielectric Relaxor Behavior in PVDF-Based Copolymer and Terpolymer Films. *AIP Adv.* **2018**, *8*, No. 045204.

(17) Veres, J.; Ogier, S.; Lloyd, G.; de Leeuw, D. M. Gate Insulators in Organic Field-Effect Transistors. *Chem. Mater.* **2004**, *16*, 4543−4555.

(18) Asadi, K. Resistance Switching in Two-Terminal Ferroelectric-Semiconductor Lateral Heterostructures. *Appl. Phys. Rev.* **2020**, *7*, No. 021307.

(19) Zhao, D.; Lenz, T.; Gelinck, G. H.; Groen, P.; Damjanovic, D.; de Leeuw, D. M.; Katsouras, I. Depolarization of Multidomain Ferroelectric Materials. *Nat. Commun.* **2019**, *10*, No. 2547.

(20) Pipertzis, A.; Asadi, K.; Floudas, G. P(VDF-TrFE) Copolymer Dynamics as a Function of Temperature and Pressure in the Vicinity of the Curie Transition. *Macromolecules* **2022**, *55*, 2746−2757.

(21) Anwar, S.; Pinkal, D.; Zajaczkowski, W.; Von Tiedemann, P.; Sharifi Dehsari, H.; Kumar, M.; Lenz, T.; Kemmer-Jonas, U.; Pisula, W.; Wagner, M.; Graf, R.; Frey, H.; Asadi, K. Solution-processed transparent ferroelectric nylon thin films. *Sci. Adv.* **2019**, *5*, No. eaav3489.

(22) Anwar, S.; Jeong, B.; Abolhasani, M. M.; Zajaczkowski, W.; Hassanpour Amiri, M.; Asadi, K. Polymer field-effect transistor memory based on a ferroelectric nylon gate insulator. *J. Mater. Chem. C* **2020**, *8*, 5535−5540.